Static and Dynamic Study of Disaccharides Trehalose, Maltose and Sucrose

Silvana C. Pamies, André N. Petelski, Eduardo A. Castro & Gladis L. Sosa

VOLUME 27, NUMBER 6

STRUCTURAL CHEMISTRY

Computational and Experimental Studies of Chemical and Biological Systems
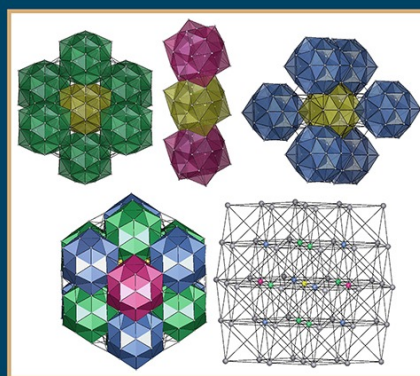
In this Issue:
Special Collection of Contributions Honoring Vladimir Ya. Shevchenko
and
Other Contributions

Springer

ONLINE FIRST

Springer

Springer

CrossMark

ORIGINAL RESEARCH

Static and Dynamic Study of Disaccharides Trehalose, Maltose and Sucrose

Silvana C. Pamies[1] · André N. Petelski[1,2] · Eduardo A. Castro[3] · Gladis L. Sosa[1,2]

Abstract In this work, electronic structure calculations and Molecular Dynamics (MD) simulations were performed in order to carry out a static and dynamic study of disaccharides, trehalose, sucrose and maltose. These three disaccharides share the same chemical formula and the same number of OH groups; however, it has been widely shown that trehalose has a superior ability to protect biological structures. In order to contribute to the understanding of the factors that determine this ability of trehalose, in this work a comparative study of the three disaccharides in gas phase and dilute aqueous solution is performed. A detailed analysis of hydrogen bonds (HBs) was carried out using Quantum Theory of Atoms In Molecules (QTAIM) on wave functions obtained at B3LYP/ 6-311++G** level. Besides, stereoelectronic effects were examined by Natural Bond Orbital (NBO) analysis. In addition, the intra- and intermolecular HB interactions in MD runs of infinitely dilute aqueous solution of sugars have been monitored. Results show that the three disaccharides form a significant number of HBs of C-H⋯O type, mainly in trehalose. An intermolecular bond of this type determines the conformational rigidity of trehalose in solution which contributes to stabilize a clam shell conformation as the one observed in the crystal. In this disaccharide, hydrogen bonds are more labile, showing a quickly exchange of the water molecules that form these HBs. This fact slows down ice formation and could be the explanation for trehalose capabilities as a cryoprotectant.

Keywords Bioprotection · Disaccharides · Anomeric effect · QTAIM · Molecular dynamics

Introduction

It has been observed [1] that certain organisms, called anhydrobiotic, when subjected to severe dehydration conditions and high temperatures, after synthesizing a large amount of saccharides, enter in a state of suspended animation in which their growth, reproduction and metabolism temporarily cease, and in which they may remain for long periods. When the environmental conditions become favorable, these organisms recover their normal metabolic activity. The synthesis of saccharides has been identified as a key factor of this phenomenon [2, 3], which is called cryptobiosis and has led to a great number of researches on the capacity of saccharides, particularly trehalose, as bioprotector agents [4–10]. The trehalose naturally occurs as α-D-glucopyranosyl-(1, 1)-α-D-glucopyranoside, which is the conformation of less energy among three possible isomers (α,α-; α,β-; β,β-). Moreover, it is a non-reductor sugar, since the glycosidic linkage involves the OH groups of the two anomeric carbons. From a thermodynamic and kinetic point of view, the trehalose is the most stable natural disaccharide. The glycosidic linkage energy is very low (less than -4.2 kJ/mol) when it is compared to the other disaccharide (the sucrose glycosidic linkage energy is +113 kJ/mol) [11]. It has also been shown that trehalose is

✉ Gladis L. Sosa
glsosa@frre.utn.edu.ar

1   Grupo de Investigación en Química Teórica y Experimental (QUITEX), Departamento de Ingeniería Química, Facultad Regional Resistencia, Universidad Tecnológica Nacional, French 414, H3500CHJ Resistencia (Chaco), Argentina

2   Instituto de Química Básica y Aplicada del Nordeste Argentino IQUIBA-NEA (UNNE, CONICET), Avenida Libertad 5460, 3400 Corrientes, Argentina

3   Instituto de Investigaciones Fisicoquímicas Teóricas y Aplicadas INIFTA (UNLP, CCT La Plata CONICET), Diag. 113 y 64, C.C. 16, Suc.4, 1900 La Plata, Argentina

Springer

able to act as a protector against physical stress caused by desiccation, osmotic changes, cold, heat and the presence of heavy metals [12–14]. In the absence of water, it keeps the fluid lipid phase separation preventing rupture and disaggregation of the membranes [15]. It effectively prevents the Maillard [16] reactions that occur between a reducing sugar and the amino group of amino acids. These properties of trehalose have numerous applications in the medical, food, cosmetic and pharmaceutical industries [17–19].

The molecular mechanism by which trehalose, and sugars in general, are able to stabilize and protect labile biomolecules is not fully understood, and it remains the subject of intense scientific activity [20–27]. In order to contribute to the understanding of this mechanism, in the current research, a static and dynamic study of the disaccharides trehalose (dihydrate and anhydrous), maltose (4-O-α-D-glucopyranosil-β-D-glucopyranoside) and sucrose (α-D-glucopyranosil-β-D-fructofuranoside) is performed. From a static point of view, the electronic structure of the sugars was analyzed in the framework of the Quantum Theory of Atoms In Molecules (QTAIM) developed by Bader [28]. Then, by Natural Bond Orbital (NBO) [29] analysis, interactions of charge transfer between donor and acceptor orbitals were evaluated and the anomeric and exo-anomeric effects examined and quantified. Finally, molecular dynamics (MD) simulations in vacuum and in infinitely dilute aqueous solution were also employed to examine the solvent effect and the characteristics of hydration of sugars. In the analysis of sugar-water interactions, special attention has been given to hydrogen bonds (HBs) of the type C-H⋯O. The study of these HBs, due to their greater lability (i.e. lower energetic requirement for their formation and/or breaking), greater angular flexibility (since they are less directional), and the possibility for water molecules involved to form bifunctional HBs, can give us further insight about what happens during the process of interest.

The results of this research are presented in two parts. In the first part, we present a study by electronic structure methods using the QTAIM and NBO analysis. In the second part, MD simulations of dilute aqueous solutions of sugars are carried out, and the interactions with water are analyzed.

Computational Details

Static study

The initial structures of the disaccharides were obtained from crystallographic data base [30–33]. In the case of trehalose, the two crystalline forms reported in the literature and the anhydrous form obtained by removing water molecules were analyzed. The geometries were optimized without any restriction using the combined Becke's three parameter exchange functional, the gradient corrected functional of Lee, Yang and Parr (B3LYP functional) [34, 35] and 6-311++G** basis set. The minimum energy nature of the optimized structures was verified using the vibrational frequency analysis. All of these electronic structure calculations were performed with the Gaussian 03 suite of programs [36].

The optimized geometries were then used to perform NBO analysis from NBO 3.1 program [37] as implemented in Gaussian 03. QTAIM calculations were carried out using wave functions generated at the B3LYP/6-311++G** level with the AIMALL [38] and MULTIWFN [39] software.

QTAIM analysis

The QTAIM has proven to be a useful and successful tool to classify and to characterize the different types of chemical bonds and, currently, it is used universally as a test of the existence of bonding interactions. Some aspects of this theory are briefly described below.

Brief outline of the QTAIM method In the QTAIM the properties of the electron density distribution of a molecule are based on the gradient vector field of the electron density $\nabla\rho(\mathbf{r})$, and the Laplacian of the electron density $\nabla^2\rho(\mathbf{r}_c)$. An atom in a molecule is defined as a region of real three-dimensional space bounded by a zero-flux surface. The points on this surface satisfy the zero-flux condition, $\nabla\rho(\mathbf{r})\cdot n(\mathbf{r}) = 0$ where $n(\mathbf{r})$ is the unit vector normal to the surface at $\mathbf{r}$. Two interacting atoms in a molecule creating a critical point in the electron density, where $\nabla\rho = 0$, which is called a bond critical point (BCP), and its coordinates, are denoted by $\mathbf{r}_c$. The pairs of gradient paths that originate at a BCP and terminate at neighboring nuclei define a line called an atomic interaction line, through which electron distribution, $\rho(\mathbf{r})$, is a maximum with respect to any neighboring line. The presence of such a line, linking two nuclei in a molecule, which exists in equilibrium geometry, implies that two atoms are bonded to another and in this instance this line is called a bond path. The network of bond paths for a molecule in a given nuclear configuration defines the molecular graph, which essentially is the union of the closures of the bond paths, and it usually corresponds to the commonly drawn chemical bond network. Different local topological properties calculated at BCP allow distinguishing between shared and closed-shell interactions. Other critical points of interest are: nuclear critical point NCP, generally located at the positions of the nuclei, ring critical point, RCP associated to a ring structure and cage critical point CCP, associated with a cage structure.

NBO analysis

In the NBO analysis [29], the electronic wave function is interpreted in terms of a set of occupied Lewis and a set of unoccupied non-Lewis localized orbitals. The interactions

between these orbitals represent the deviation of molecule from the Lewis structure and can be used as the measure of delocalization. The strengths of these interactions are quantitatively estimated by means of the second-order perturbation interaction energy, $E^{(2)}$.

Dynamic study

The optimized structure of each disaccharide was solvated with 1500 water molecules TIP3P [40] in an octahedral box. Point charges on the atomic nuclei were fitted by RESP [41] using Gaussian 03 at HF/6-31G* level of theory. MD simulations were performed with the AMBER 11 [42] software suite using GAFF and ff99SB force fields. Simulations were preceded by 2 stages of energy minimization using Steepest Descent and Conjugate Gradient methods. The first stage was performed using harmonic constraints of force on the atoms of sugars, and the second one without restrictions. The resulting systems of minimum potential energy were subjected to 500 ps of MD under constant volume conditions until 300 K with movement restrictions on the same molecules as in the first stage of minimization. Then, the system was equilibrated in the NPT ensemble at 300 K and 1 atm with no restrictions on the molecules, during 10 ns. Constant temperature and pressure were satisfied by Langevin [43] coupling algorithm, and all bond lengths involving hydrogen atoms were restricted with the SHAKE [44] algorithm. Long-range electrostatic interactions were calculated using the particle-mesh Ewald (PME) [45] method, while van der Waals (vdW) interactions were calculated using the 6-12 Lennard-Jones potential. The cutoff distance for non-bonded van der Waals interactions was set to 10 Å. The equations of motion were integrated with a step size of 2 fs. Data collection run was performed in the NVT ensemble during 25 ns.

Finally, in order to analyze the influence of the solvent on the geometry and HBs of the three disaccharides, 25 ns of MD runs in vacuum were also performed.

Results and discussion

Quantum Mechanics Calculations

Figure 1 shows a schematic representation of trehalose anhydrous (Fig. 1a), sucrose (Fig. 1b) and maltose (Fig. 1c) and Fig. 2 shows the two crystalline forms of trehalose dihydrate (Fig. 2a, b). The dihedral angle defining conformational flexibility around the glycosidic bond, Φ, Ψ and those that define the conformations of hydroxymethyl groups, ω, ω' and χ are also indicated.

The selected geometric parameters calculated at the B3LYP/6-311++G** level are given in Table 1. Experimental values obtained by X-ray diffraction on the
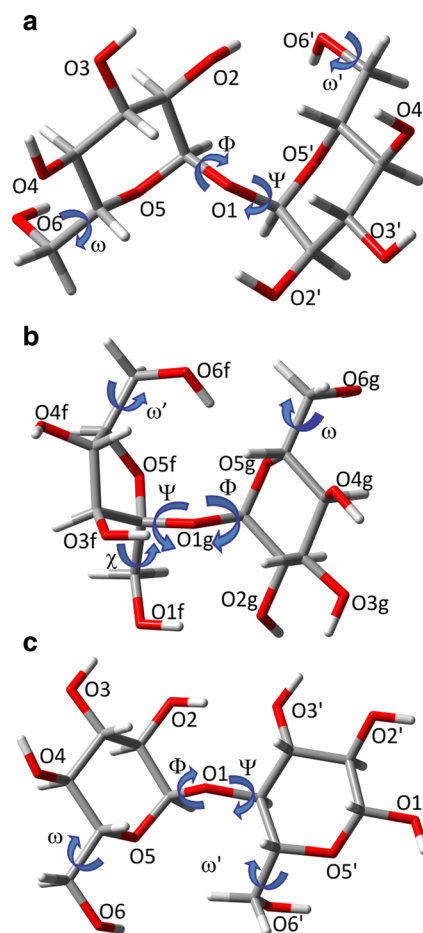

Fig. 1. Molecular structures of: **a** trehalose, **b** sucrose and **c** β-maltose. The numbering of the oxygen atoms is indicated. Torsion angles are defined as: Φ = O5-C1-O1-C1' and Ψ = C1-O1-C1'-O5'; Φ = O5g-C1g-O1g-C2f and Ψ = C1g-O1g-C2f-O5f; Φ = O5-C1-O1-C4' and Ψ = C1-O1-C4'-C5' in trehalose, sucrose and maltose respectively. The conformations of the hydroxymethyl groups are described by the torsional angles: ω = O5-C5-C6-O6 and ω' = O5'-C5'-C6'-O6' in trehalose and maltose and ω_g = O5g-C5g-C6g-O6g, ω_f = O5f-C5f-C6f-O6f and χ_f = O1f-C1f-C2f-O5f in sucrose

crystal structures are given between parentheses. Comparing both values, the calculated and experimental ones, it is observed that the geometry that adopts the sucrose, maltose and trehalose dihydrate-1 in gaseous phase is similar to what they exhibit on the crystal. For instance, the minimum energy geometry of sucrose in gas phase is characterized by intersaccharidic torsion angles Φ/Ψ ≈ 107.3°/-46.1° that differ little from those found in the crystal (+108.3°and -44.7°, respectively). In contrast, in anhydrous trehalose and trehalose dihydrate-2 (Fig. 2b), Φ deviates about 30 degrees from the value in the respective crystals. Particularly in the case of the anhydrous form, Φ and Ψ differ significantly from the values reported for the crystal of Φ/Ψ = 70,1°/55.1° [46] and Φ/Ψ = 60.8°/60.1° [47] and from other informed value considered as a minimum of energy of Φ/Ψ = 72.6°/72.6° [48]. However, it is important to take into consideration that the
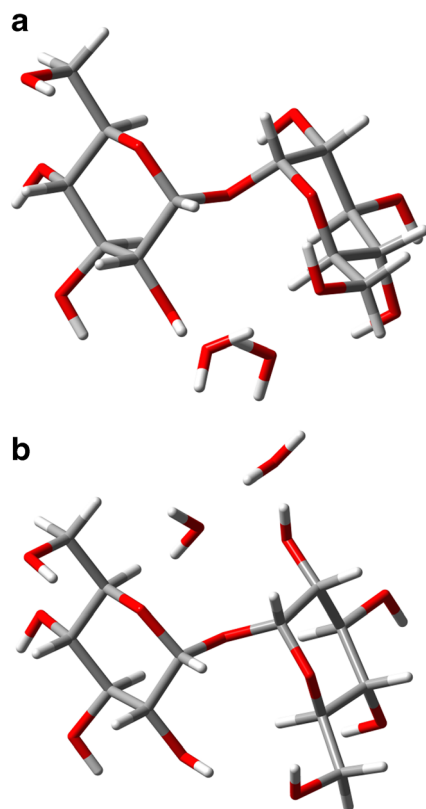
Fig. 2. Molecular structures of: **a** trehalose dihydrate-1 and **b** trehalose dihydrate-2

anhydrous structure analyzed herein was obtained by removing water molecules of the hydrated structure. In addition, the

conformation of lowest energy reported by Nunes et al. was also taken as the starting conformation for subsequent energy minimization. Nevertheless, this structure has converged to another conformer ($\Phi/\Psi \approx 74.1°/80.0°$) that is 1.4 kcal/mol less stable than that obtained by us.

Regarding to ω, ω' and χ angles, it is observed that calculated and experimental values differ significantly in the case of anhydrous trehalose and trehalose dehydrates. However, these dihedrals adopt geometry similar to the crystal in sucrose and maltose. With respect to θ angle, the biggest differences with respect to crystal values correspond to sucrose and maltose, and it should also be noted its relatively large deviation with respect to standard (tetrahedral) value, 109.5°.

Differences between the endocyclic oxygen-anomeric carbon bond lengths and the exocyclic oxygen-anomeric carbon bond lengths, are related to stereoelectronic effects and will be discussed later.

Topological Analysis

In Fig. 3, the molecular graphs of anhydrous and dihydrate trehalose, maltose and sucrose, are displayed. In Table 2 the topological parameters calculated at BCPs are listed. The parameters reported are: the electron density, $\rho(\mathbf{r}_c)$, the Laplacian of the electron density, $\nabla^2\rho(\mathbf{r}_c)$, the ellipticity, ($\varepsilon = \lambda_1/\lambda_2 - 1$) and kinetic energy densities, $G(\mathbf{r}_c)$, potential energy, $V(\mathbf{r}_c)$, and total energy, $H(\mathbf{r}_c) = G(\mathbf{r}_c) + V(\mathbf{r}_c)$. Since in literature it is well established that there is an almost linear correlation between the value of density at BCPs and the strength of the

Table 1. Selected geometric parameters calculated at the B3LYP/6-311++G** level

	Anhydrous trehalose[1]	Trehalose dihydrate-1[2]	Trehalose dihydrate-2[3]	Sucrose[4]	β-Maltose[5]
d(C1-O1)/d(C1g-O1)	1.4237 (1.4278)	1.4154 (1.4156)	1.4404 (1.4165)	1.4129 (1.4286)	1.4237 (1.4144)
d(C1'-O1)/d(C2f-O1)/ d(C1'-O1')	1.4210 (1.4237)	1.4229 (1.4271)	1.4640 (1.4197)	1.4492 (1.4357)	1.3951 (1.3898)
d(O5-C1)/d(O5g-C1g)	1.4061 (1.4004)	1.4101 (1.4224)	1.4582 (1.4230)	1.4160 (1.4147)	1.4087 (1.4036)
d(O5'-C1')/d(O5f-C2f)	1.4122 (1.4047)	1.4150 (1.4079)	1.4449 (1.4076)	1.4083 (1.4093)	1.4204 (1.4182)
d(O5-C5)/d(O5g-C5g)	1.4491 (1.4447)	1.4453 (1.4289)	1.5089 (1.4378)	1.4518 (1.4452)	1.4459 (1.4338)
d(O5'-C5')/d(O5f-C5f)	1.4457 (1.4590)	1.4429 (1.4258)	1.4862 (1.4235)	1.4572 (1.4545)	1.4380 (1.4230)
O5-C1-O1/O5g-C1g-O1	111.55 (111.42)	112.1 (112.1)	110.7 (111.9)	111.4 (110.1)	111.3 (110.7)
O5'-C1'-O1/O5f-C2f-O1	110.81 (112.24)	111.5 (111.3)	108.7 (111.3)	111.4 (110.9)	108.9 (108.1)
Φ	99.9 (70.1)	80.5 (74.9)	106.3 (75.0)	107.3 (108.3)	113.4 (121.7)
Ψ	69.8 (55.1)	68.9 (61.9)	64.5 (61.8)	-46.1 (-44.7)	-109.0 (-107.8)
Ω	-57.7 (-61.0)	-58.2 (-75.7)	-58.5 (-75.3)	-60.5 (-56.5)	59.0 (59.2)
ω'/ω_f	60.6 (-63.4)	58.9 (70.0)	58.1 (69.9)	-64.2 (-70.1)	-61.7 (-62.4)
χ_f				175.1 (171.1)	
*θ	114.3 (113.0)	115.4 (115.8)	114.8 (115.7)	118.3 (113.4)	119.3 (117.9)

Distances are in angstroms and angles are in degrees. Values in parentheses correspond to the structures obtained by X-ray diffraction. The torsional angles are defined in Fig. 1

*θ angle of the glycosidic bond

[a] Database code Cambridge Structural Database (CSD): DEKYEX01, from [46]

[b] Database code CSD: TREHAL01, from [30]

[c] Database code CSD: TREHAL03, from [31]

[d] Database code CSD: SUCROS01, from [32]

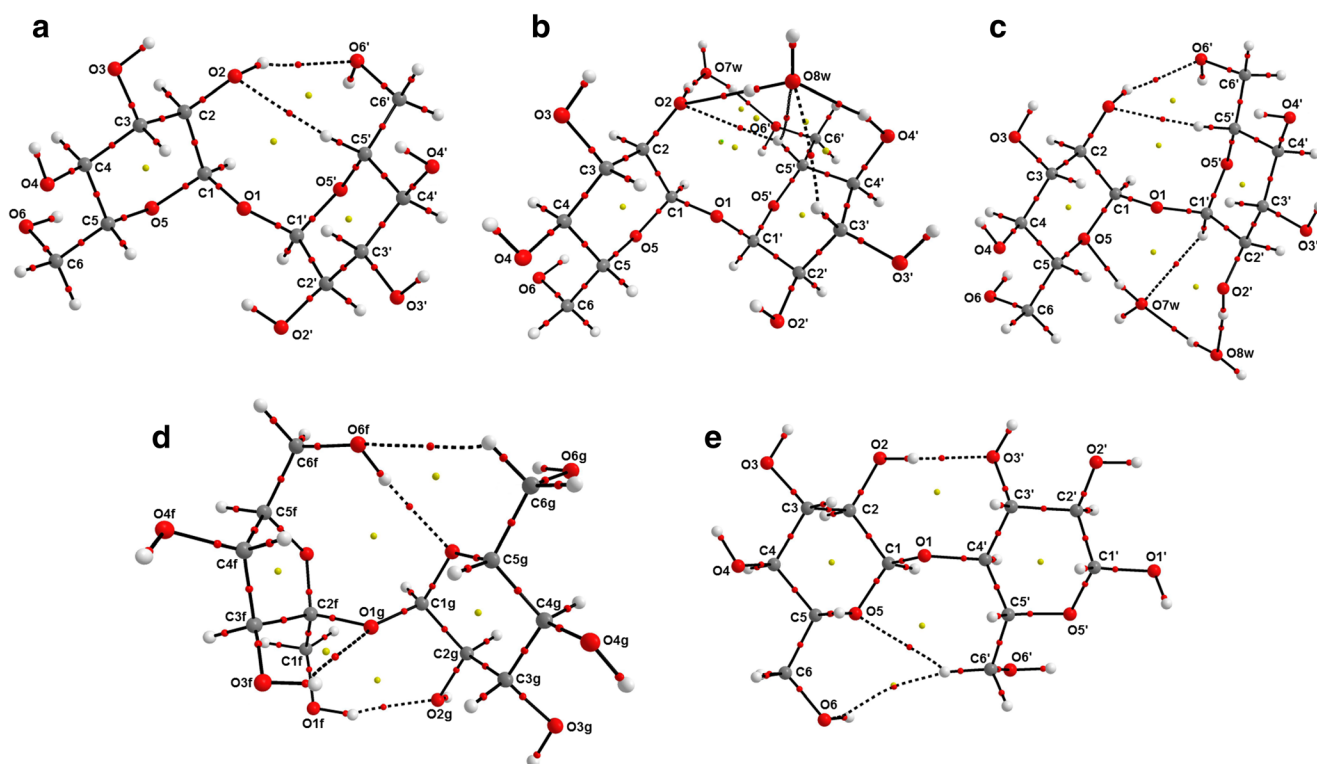[e] Database code CSD: MALTOS11, from [33]

Fig. 3. Molecular graphs: **a** anhydrous trehalose; **b** trehalose dihydrate-1; **c** trehalose dihydrate-2; **d** sucrose; **e** maltose. *Small red dots* indicate bond critical points (BCP); *yellow*, ring critical points (RCP); *green*, cage critical point (CCP)

interaction [49, 50], this criterion is used to compare the strength of different HBs in the discussion that follows.

In all disaccharides the QTAIM analysis reveals the occurrence of BCPs indicating the formation of intramolecular HBs of O–H···O and C–H···O type. These HBs lead to the formation of extra rings in the structure of disaccharides. The $\rho(\mathbf{r}_c)$ ranges from 0.0038 to 0.0372 au, which compares fairly well with values reported for different HB interactions, in which this quantity was found to vary from 0.002 to 0.034 au [51]. Similarly, the $\nabla^2\rho(\mathbf{r}_c)$ ranges from 0.0138 to 0.1290 au, and it also compares satisfactorily with previous results that vary from 0.016 to 0.139 au [51].

In the case of anhydrous trehalose, an intramolecular bifunctional HB is observed. The O2 atom exhibits a dual behavior, acting as proton donor to O6' and as proton acceptor of C5'. This bifunctional HB leads to the formation of six-membered (with C6' and C5') and eight-membered rings (involving glycosidic oxygen) closed by HBs. In the trehalose dihydrate-1, a water molecule inserts between the O2 and O6' and forms an intermolecular bifunctional HB, O7w acts as proton acceptor of O2 and as proton donor of O6': O2-H···(O7w–H)···O6'. The highest values of density are observed at these BCPs ($\rho(\mathbf{r}_c) = 0.0372$ au and $\rho(\mathbf{r}_c) = 0.0351$ au, respectively); furthermore, the potential energy density is of greater magnitude than the kinetic energy density leading to negative values of total energy density, and indicating the greatest strength of these HBs. The O8w of another water

Table 2. Topological parameters calculated at C–H···O and O–H···O BCPs for all disaccharides

	$\rho(\mathbf{r}_c)$	$\nabla^2\rho(\mathbf{r}_c)$	ε	$G(\mathbf{r}_c)$	$V(\mathbf{r}_c)$	$H(\mathbf{r}_c)$
Anhydrous trehalose						
C5'–H···O2	0.0132	0.0427	0.1307	0.0094	-0.0081	0.0013
O2–H···O6'	0.0153	0.0489	0.0717	0.0109	-0.0096	0.0013
Trehalose dihydrate 1						
C5'–H···O8w	0.0066	0.0236	0.7825	0.0050	-0.0042	0.0009
C5'–H···O2	0.0068	0.0202	0.0244	0.0045	-0.0040	0.0005
C3'–H···O8w	0.0069	0.0226	0.4086	0.0049	-0.0042	0.0007
O4'–H···O8w	0.0253	0.0926	0.0986	0.0212	-0.0192	0.0020
O8w–H···O2	0.0296	0.1062	0.0590	0.0252	-0.0239	0.0013
O7w–H···O6'	0.0351	0.1167	0.0355	0.0294	-0.0297	-0.0003
O2–H···O7w	0.0372	0.1290	0.0540	0.0328	-0.0333	-0.0005
Trehalose dihydrate 2						
C1'–H···O7w	0.0050	0.0178	0.1443	0.0038	-0.0031	0.0007
C5'–H···O2	0.0126	0.0406	0.1272	0.0089	-0.0077	0.0012
O2–H···O6'	0.0158	0.0507	0.0661	0.0113	-0.0099	0.0014
O2'–H···O8w	0.0297	0.1101	0.0601	0.0260	-0.0245	0.0015
O7w–H···O5	0.0303	0.1052	0.0513	0.0254	-0.0244	0.0009
O8w–H···O7w	0.0308	0.1116	0.0814	0.0266	-0.0253	0.0013
Sucrose						
C6g–H···O6f	0.0069	0.0255	0.2845	0.0054	-0.0044	0.0010
O3f–H···O1g	0.0195	0.0847	0.6381	0.0187	-0.0162	0.0025
O6f–H···O5g	0.0209	0.0738	0.0697	0.0166	-0.0148	0.0018
O1f–H···O2g	0.0220	0.0797	0.0538	0.0180	-0.0161	0.0019
Maltose						
O2–H···O3'	0.0231	0.0871	0.0883	0.0195	-0.0172	0.0023
C6'–H···O5	0.0081	0.0246	0.1657	0.0055	-0.0048	0.0007
C6'–H···O6	0.0038	0.0138	7.6333	0.0027	-0.0020	0.0007

All quantities are in atomic units. Symbols are explained in the text

molecule is tetra-coordinate and forms a net of interconnected HBs, O8w-H···O2, C5'-H···O8w, C3'-H···O8w and O4'-H···O8w. Besides, the intramolecular HB, C5'-H···O2 found in the anhydrous form also occurs in this hydrate, although the density is partitioned between the C5'-H···O8w ($\rho(\mathbf{r}_c)$ = 0.0066 au) and C5'-H···O2 ($\rho(\mathbf{r}_c)$ = 0.0068 au) HBs. In trehalose dihydrate-2, the two water molecules are bonded together by HB, O7w···H-O8w and simultaneously form the HBs, C1'–H···O7w–H···O5 and O2'–H···O8w with trehalose molecule. Again, the intramolecular C5'–H···O2 HBs, which was found both in the anhydrous and the dihydrate-1 form, occur in this hydrate, as well as it does the HB O2-H···O6', although in the dihydrate-1 a water molecule is acting as a bridge between O2 and O6'. It is also important to note that the glycosidic oxygen is not involved in HBs in any of the forms of trehalose.

Sucrose is the only case in which the exocyclic oxygen participates in a HB, in the same way it is the disaccharide with the greatest number of intramolecular HBs. These HBs give rise to formation of four rings and their associated RCPs (see Fig. 3d). One is a bifunctional HB, C6g–H···O6f–H···O5g, in which the O6f oxygen acts as proton donor to O5g oxygen and as acceptor to C6g. The other two HBs, despite being of O–H···O type, have relatively low density values: 0.022 au and 0.0195 au for O1f–H···O2g and O3f–H···O1g HBs respectively. It is important to note that O6f–H···O5g and O1f–H···O2g HBs are the same ones that have been observed in the crystalline sucrose [32] although QTAIM analysis reveals a more complex structure of intramolecular HBs. Something similar occurs in maltose. The crystalline β-maltose [33] forms one intramolecular HB O2–H···O3', while our gaseous phase calculations reveal a relatively strong HB, O2–H···O3' ($\rho(\mathbf{r}_c)$ = 0.0231 au) and a bifurcated HB, O5···H(−C6')···O6. The bifurcated HB consists of two C–H···O nonconventional HBs, one involving the endocyclic oxygen, C6'–H···O5 ($\rho(\mathbf{r}_c)$ = 0.0081 au) and another one which is extremely weak, C6'–H···O6, as it is reflected in a very low density value ($\rho(\mathbf{r}_c)$ = 0.0038 au), high value of ellipticity (ε = 7.63) and the short distance between the BCP and the RCPs next to it (see Fig. 3e). These characteristics have been associated by Bader [28] with a bond that is close to a formation or destruction process (catastrophe points).

NBO analysis

Table 3 shows the results of the NBO analysis related to the formation of HBs. Occupation numbers for the σ(O–H)*, σ(C–H)* antibonds, occupation numbers for oxygen lone pairs, nlp and the second-order perturbation energies $E^{(2)}$ (donor → acceptor) that involve these orbitals are listed. It can be seen that the hyperconjugative charge transfer interactions (HCTI) related to the formation of the C–H···O HBs are smaller (in some cases negligibly) than the ones corresponding to

Table 3. NBO analysis of hydrogen bonds: occupation numbers for the $\sigma_{O-H}^*/\sigma_{C-H}^*$ antibonds and n_{lp} lone pairs, and the second-order perturbation energies E^2 (donor → acceptor: $n_{lp} \rightarrow \sigma_{O-H}^*/\sigma_{C-H}^*$)

	E^2 (lpO → σ*)	n_{lp}	σ*
Anhydrous Trehalose			
lp(O6') → σ*(O2–H)	2.70	1.9544	0.0164
lp(O2) → σ*(C5'–H)	1.04	1.9502	0.0374
Trehalose dihydrate 1			
lp(O2) → σ*(C5'–H)	0.66	1.9470	0.0369
lp(O2) → σ*(O8w–H)	5.32		0.0243
lp(O6') → σ*(O7w–H)	12.64	1.9421	0.0329
lp(O8w) → σ*(C3'–H)	0.23	1.9782	0.0387
lp(O8w) → σ*(C5'–H)	0.28		0.0369
lp(O8w) → σ*(O4'–H)	8.61		0.0249
lp(O7w) → σ*(O2–H)	16.62	1.9627	0.0382
Trehalose dihydrate 2			
lp(O7w) → σ*(C1'–H)	0.35	1.9943	0.0313
lp(O2) → σ*(C5'–H)	0.90	1.9498	0.0373
lp(O6') → σ*(O2–H)	2.99	1.9539	0.0175
lp(O8w) → σ*(O2'–H)	10.98	1.9750	0.0260
lp(O5) → σ*(O7w–H)	4.84	1.9140	0.0270
lp(O7w) → σ*(O8w–H)	11.37	1.9726	0.0243
Sucrose			
lp(O6f) → σ*(O6g–H)	–	1.9505	0.0239
lp(O5g) → σ*(O6f–H)	2.780	1.9079	0.0235
lp(O2g) → σ*(O1f–H)	3.230	1.9535	0.0196
lp(O1g) → σ*(O3f–H)	1.260	1.8981	0.0127
Maltose			
lp(O3') → σ*(O2–H)	4.85	1.9539	0.0262
lp(O5) → σ*(C6'–H)	–	1.9063	0.0207
lp(O6) → σ*(C6'–H)	–	1.9540	0.0207

the O–H···O HBs, indicating that the HCTI do not play an important role in the formation of these weak C–H···O HBs.

In line with the QTAIM analysis, in trehalose dihydrate 1, two strong HICT are observed, both of them involving water molecules that bind to O2 and O6' (lp(O7w) → σ*(O2–H) = 16.62 kcal/mol and lp(O6') → σ*(O7w–H) = 12.64 kcal/mol). Similarly, in trehalose dihydrate 2, the strongest HICT are those which are related to intermolecular HBs with water (lp(O8w) → σ*(O2'–H) = 10.98 kcal/mol and lp(O7w) → σ*(O8w–H) = 11.37 kcal/mol).

In sucrose, these HICT are less important than in the dihydrate trehaloses, though stronger than in the anhydrous trehalose. Finally, in maltose, the only HICT observed is related to HB, O2–H···O3', (lp(O3') → σ*(O2–H) = 4.85 kcal/mol).

Anomeric and exo-anomeric Effects by NBO analysis The anomeric effect was initially defined [52] as the preference for an electronegative substituent at the anomeric carbon in a carbohydrate, to be in an axial rather than equatorial

orientation, in contrast to the expected based on steric interactions. This effect is now considered to be a special case of a general preference (the generalized anomeric effect) for synclinal (gauche) conformations about the bond C–Y in the systems X–C–Y–C in which X and Y are heteroatoms having nonbonding electron pairs. According to the stereoelectronic model, this preference has its origin in a stabilizing interaction (hyperconjugative delocalization) between a nonbonding electron pair on the heteroatom (the endocyclic oxygen in a sugar ring) and the antibonding orbital, σ^*, for the (exocyclic) C–X bond, which is possible only in the axial direction. Delocalization is expected to result in the lengthening of the exocyclic C–O bond, a concomitant shortening of the endocyclic C–O bond and opening of the O–C–O bond angle with respect to "standard" (tetrahedral) values due to the reduced and enhanced p-character of the endocyclic and exocyclic C–O bonds, respectively.

In alkyl glycopyranosides the anomeric effect operates at two sites, along the endocyclic C1–O bond (endo-anomeric effect) and along the exocyclic C1-O bond (exo-anomeric effect).

In Table 4, the hyperconjugative interactions of charge transfer (HICT) related to these effects in the three disaccharides are reported. It can be seen that in the anhydrous trehalose, as expected, the HICT lp(O1) → σ^*(C1–O5) and lp(O1) → σ^*(C1'–O5') related to the exo-anomeric effect, are of almost same magnitude and the two HICT, lp(O5) → σ^*(C1–O1) and lp(O5') → σ^*(C1'–O1) related to endo-anomeric effect differ relatively little, 1.6 kcal/mol. The total exo-anomeric effect (25 kcal/mol) is virtually offset by total endo-anomeric effect (25.6 kcal/mol). As a result, C1–O1/C1'–O1 bond distances are similar to C1–O5/C1'–O5'. The same occurs in trehalose dihydrate-1, while in dihydrate-2 the exo-anomeric effect is 7 kcal/mol greater than the endo-anomeric effect, and C1–O1 and C1'–O1 bond distances are shorter than C1–O5 and C1'–O5' respectively. These results also show that the stabilization due to delocalization of electronic charge in the dihydrate-1 is higher than in dihydrate-2 and it is in line with the HF energies for these hydrates. In sucrose, the total endo-anomeric effect is 8 kcal/mol greater than the total exo-anomeric effect. The exo-anomeric effect towards fructose ring is about 5 kcal/mol lower than towards glucose ring, while the energy corresponding to HICT, lp(O5f) → σ^*(C2f–O1g) is the highest of all (16.27 kcal/mol). Thus, it can be seen in Table 1 that in fructose ring O5f–C2f bond is shorter than O1–C2f one while in glucose ring the differences in the bond distances O1-C1 and O5–C1 agree well what is expected for the exo-anomeric effect. Maltose also exhibits two exo-anomeric effects, one involving exocyclic oxygen, lp(O1) → σ^*(C1–O5) and another one involving oxygen O1', lp(O1') → σ^*(C1'–O5'). On the other hand, as expected considering that the glycosidic linkage in the maltose is $\alpha(1 \rightarrow 4)$, it exhibits a unique endo-anomeric effect, lp(O5) → σ^*(C1–O1), 1.8 Kcal greater than the corresponding exo-anomeric. This HICT causes a shortening of the O5–C1 bond and a lengthening of the C1–O1 bond (see Table 1).

Table 4. NBO analysis: occupation numbers for the σ^*_{C-O} antibonds and n_{lp} lone pairs, and the second-order perturbation energies E^2 (donor → acceptor) corresponding to $n_{lp} \rightarrow \sigma^*_{C-O}$ HICTs

	E^2 (lpO → σ^*)	n_{lp}	σ^*
Anhydrous Trehalose			
lp(O1) → σ^*(C1'–O5')	12.31	1.8894	0.0556
lp(O1) → σ^*(C1–O5)	12.24		0.0523
lp(O5) → σ^*(C1–O1)	13.61	1.9047	0.0657
lp(O5') → σ^*(C1'–O1)	11.99	1.9085	0.0616
Trehalose dihydrate 1			
lp(O1) → σ^*(C1'–O5')	13.09	1.8877	0.0548
lp(O1) → σ^*(C1–O5)	11.95		0.0546
lp(O5) → σ^*(C1–O1)	12.84	1.9065	0.0630
lp(O5') → σ^*(C1'–O1)	11.69	1.9098	0.0616
Trehalose dihydrate 2			
lp(O1) → σ^*(C1'–O5')	14.60	1.8780	0.0645
lp(O1) → σ^*(C1–O5)	12.35		0.0557
lp(O5) → σ^*(C1–O1)	8.51	1.9140	0.0541
lp(O5') → σ^*(C1'–O1)	11.67	1.9104	0.0610
Sucrose			
lp(O1g) → σ^*(C1g–O5g)	12.10	1.8981	0.0570
lp(O1g) → σ^*(C2f–O5f)	6.83		0.0533
lp(O5f) → σ^*(C2f–O1g)	16.27	1.8923	0.0923
lp(O5g) → σ^*(C1g–O1g)	11.19	1.9079	0.0611
Maltose			
lp(O1) → σ^*(C1–O5)	10.95	1.9027	0.0534
lp(O1') → σ^*(C1'–O5')	13.44	1.9314	0.0593
lp(O5) → σ^*(C1–O1)	12.76	1.9063	0.0628

Molecular Dynamics

Structural analysis

The conformational mobility of the three disaccharides in solution was studied by observing the time variation of the main torsion angles, Φ, Ψ, ω, ω' and χf, described in Section Quantum Mechanics Calculations. Plots of the trajectories and statistical analysis are shown in Figs. 4a–i and in Table 5, respectively.

It can be seen that in trehalose Φ and Ψ average dihedrals are identical (Fig. 4a), and so are ω and ω' (Figs. 4d, g), consistent with the high symmetry of trehalose. The values of these torsion angles agree well with the experimental data which provide validation for the force field and the simulation methodology employed. The high percentage of occupancy and relatively low standard deviation, observed in Φ and Ψ torsion angles, show the rigidity of trehalose around glycosidic linkage. This rigidity is also observed in vacuum (Fig. 4a) as these dihedrals take values close to the ones found in solution.
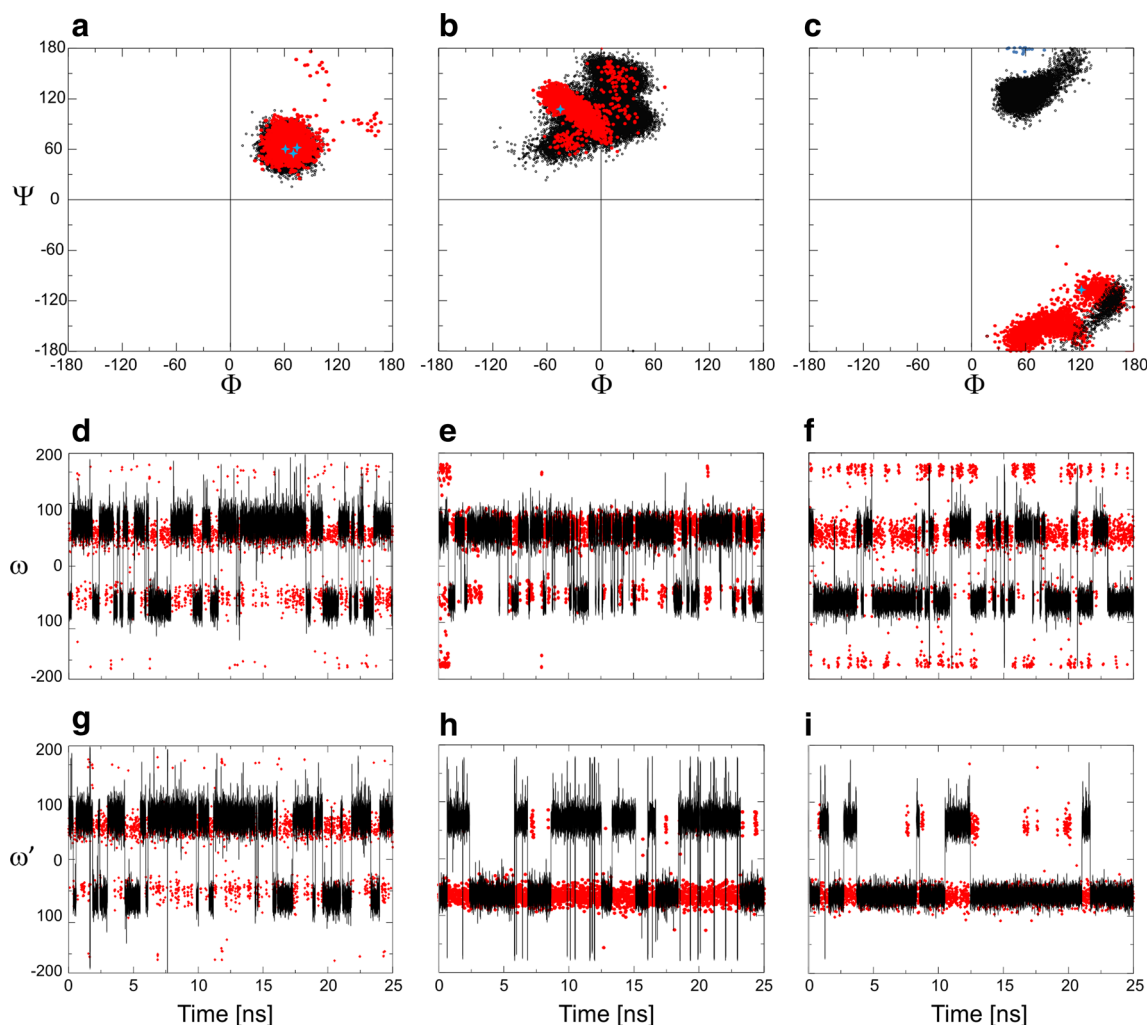
Fig. 4. Variations of dihedral angles along the MD trajectories: Ψ vs. Φ in vacuum (*red*) and in aqueous solution (*black*) of **a** Trehalose, **b** Sucrose and **c** Maltose. *Small blue stars* indicate the crystal structure values. ω angles of **d** trehalose, **e** sucrose and **f** maltose; and ω' angles of **g** trehalose; **h** sucrose; **i** maltose

In sucrose, however, important fluctuations are observed taking Φ and Ψ other values rather than those reported in the crystalline state (Φ = 108.3° and Ψ = -44.7°). Dihedral Φ increases to an average value of 117° while Ψ takes a positive value of 20.9°. Ψ also adopts a value very close to the one in the crystal (-43.6°) in several instances along the trajectory with an occupancy of 12.4%. This result indicates that sucrose is less rigid than trehalose and is consistent with the reported one by Choi et al. [53] who, when comparing the time-correlation functions for collected motions of glycosidic linkage of different sugars, found that the dynamic motion occurs more slowly in trehalose than in the other sugars in aqueous solution. In contrast, values from MD in vacuum for Φ are similar to the crystal ones (115.8° and occupancy of 80.9%) while Ψ exhibits much more mobility.

Maltose shows a similar behavior to the trehalose one, with high-occupancy percentages of Φ and Ψ dihedrals (95.1 and 95.8% respectively) but taking a completely different conformation from the one observed in the crystal. Φ dihedral (57.8°) adopts a gauche conformation, while in the crystal structure it is of 121.7° [33]. Besides, Ψ dihedral adopts a positive anticlinal conformation (126.4°), while in the crystal structure this value is -107.7°. Analyzing the trajectories of Φ and Ψ dihedrals, it can be observed that maltose adopts the crystal like structure in two small periods of the simulation time. The average values adopted are 116.4° (occupancy 3.3%) and -125° (occupancy 2.6%) respectively. This situation, as we shall see, occurs when the HB O2-H···O3' is formed. In contrast to Φ and Ψ dihedrals, as shown in Fig. 4d–i. ω and ω' are not so affected by the solvent.

Summarizing, results from MD in vacuum and solution show that solvent practically does not perturb the trehalose structure. Contrarily, structures of maltose and sucrose are significantly affected.

Struct Chem

Table 5. Statistics of geometrical values calculated along the 25 ns of MD

Angle	Statistics	Trehalose	Sucrose	Maltose
Φ	Average	62.0	117.0	57.8
	% occupied	99.5	65.6	95.1
	Std. Dev.	10.2	19.1	10.0
Ψ	Average	62.1	20.9	126.4
	% occupied	99.4	65.5	95.8
	Std. Dev.	10.3	12.7	8.0
ω	Average	65.8	63.5	-63.2
	% occupied	65.2	71.8	64.6
	Std. Dev.	11.5	12.7	10.6
ω'	Average	65.8	67.9	-63.7
	% occupied	66.2	50.6	81.5
	Std. Dev.	11.8	11.4	9.7
χ^f	Average		58.7	
	% occupied		99.4	
	Std. Dev.		11.6	
θ	Average	115.3	119.7	118.1
	Std. Dev.	3.5	3.2	3.3

Radial Distribution Functions

In order to obtain the degree of solvation of disaccharides in infinitely dilute aqueous solutions, the radial distribution functions (RDFs) between oxygen atoms of the sugars and the water molecules were calculated. Besides, the coordination numbers derived from RDF, taking a coordination radius of
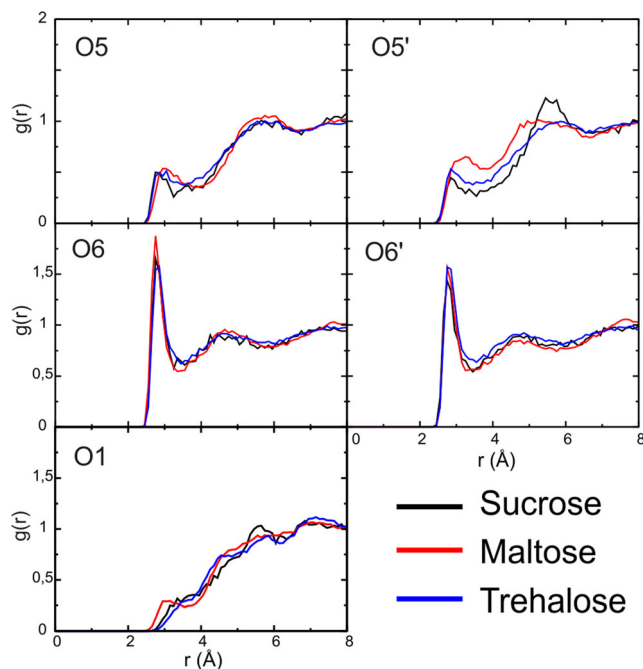
Fig. 5. Comparison of the radial distribution functions of the water oxygen atoms around five different oxygen atoms of disaccharides

Table 6. Number of water molecules in the first shell around the sugar oxygens (O_S) by integrating the O_S–O_w radial distribution function to 3.45 Å

Trehalose		Sucrose		Maltose	
Oxygen	Number	Oxygen	Number	Oxygen	Number
1	0.46	1g	0.62	1	0.82
2	3.08	2g	2.87	2	3.42
3	3.27	3g	3.51	3	3.46
4	3.02	4g	3.06	4	3.07
5	1.47	5g	1.29	5	1.52
6	3.38	6g	3.30	6	3.35
2'	3.07	1f	2.99	1'	3.69
3'	3.28	3f	2.26	2'	3.49
4'	3.01	4f	2.93	3'	2.85
5'	1.47	5f	1.17	5'	1.90
6'	3.38	6f	3.04	6'	3.04
TOTAL	28.89	TOTAL	27.04	TOTAL	30.61

3.45 Å, were obtained. Figure 5, shows the RDFs of the most significant oxygen atoms, O1, O5, O5', O6 and O6'. In Table 6 the hydration numbers are reported.

O6 and O6' oxygen atoms exhibit a typical hydrophilic hydration with small differences between the three disaccharides. The RDFs around these oxygens show a well-defined sharp first peak centered at 2.8 Å with peaks densities that range between 1.5 and 1.8, and a minimum at 3.45 Å. According to the results of Table 6, trehalose possesses a coordination number slightly greater than sucrose and maltose on these oxygen atoms. The endocyclic oxygens are poorly hydrated as can be inferred from the small peak of the first hydration shell, being maltose the one with the greatest number of hydration, of practically two water molecules, against one in trehalose and sucrose. Regarding glycosidic oxygen, an almost null hydration is observed in trehalose and sucrose, while maltose, probably due to its more open structure, presents a value nearing 1.

Comparing the total numbers of water molecules in the first hydration shell reported in Table 6, it can be seen that the degree of hydration increases in the order, sucrose <trehalose < maltose, although the differences are rather small. In the literature there is a wide range of values, experimental and theoretical ones, for this parameter [53–55]. The data reported here are in good agreement with those reported by Engelsen

Table 7. Time-averaged number of intermolecular hydrogen bonds between water molecules and disaccharides

Disaccharide	O-H···O	C-H···O	Total Number
Trehalose	17.36	12.44	29.80
Maltose	16.51	10.40	26.91
Sucrose	13.64	9.82	23.46

et al. [56] However, as it is pointed out by these authors, simulations are not able to contrast the hydration numbers of trehalose and sucrose.

Intermolecular HBs

Sugar-water interactions have been extensively studied, including different experimental techniques, MD simulations and over a wide range of concentrations and temperatures [26, 55–61]. However, in these studies, little or no attention has been given to the HBs of C-H⋯O type, despite as it has been shown, these HBs are of great importance in biological systems in which sugars exert their protective role. In this work, in addition to conventional O-H⋯O, the C-H⋯O HBs were also examined. Both types of HBs were evaluated using a geometric criterion, which is based on the distance between the donor and the acceptor oxygen, and the angle formed by the donor atom, the acceptor hydrogen and the acceptor oxygen. The cutoff distance between donor and acceptor atoms was set to 3.4 Å and the cutoff for the angle was set to 120°. Table 7 shows the number of HBs, and Figs. 6 and 7 show the average lifetime and % occupancy of O-H⋯O and C-H⋯O HBs respectively. Comparing the results obtained for the three disaccharides, it can be seen in Table 7 that trehalose forms the highest total number of HBs with water, but the lowest occupancy percentage and average lifetime. These facts indicate that trehalose also forms the weakest HBs.

The second smallest number of intermolecular HBs, but an occupancy percentage higher than the other disaccharides, is observed for maltose. Sucrose forms the lowest number of HBs, with occupancy similar to the trehalose one and a mean lifetime higher but very similar to maltose.

Intramolecular HBs

As was discussed in section Quantum Mechanics Calculations, in the gas phase trehalose forms a bifunctional intramolecular C-H⋯O HB. Thus we consider that it is important to explore intramolecular HBs in aqueous solutions. The distances between oxygen atoms of disaccharides that could be involved in an intramolecular HB, particularly those found in DFT results, were calculated and plotted as a function of the simulation time. The results are shown in Fig. 8. In addition, a more rigorous analysis is accomplished in terms of QTAIM theory. For each system, a minimum potential energy structure was extracted from the production MD simulations and all water molecules in a radius greater than 5 Å were removed. With each structure, a wave function at B3LYP/6-31G* level was generated with Gaussian 03 [36], without optimization. The electron charge density was analyzed with the Multiwfn [39] program, and the molecular graphs are shown in Fig. 9.

When considering the distances between O2/O2' and O6'/O6 oxygen atoms within a trehalose molecule they do not reach a value consistent with the formation of an HB at any point during the simulation. Conrad et al. [62] have suggested that trehalose has a tendency to form a HB between O2/O6 and O6'/O2' hydroxyls, especially at concentrated solutions (higher than 50%). In this research, as a result of the high dilution state, a notable mobility of hydroxymethyl groups has been obtained, and thus avoiding the formation of stable
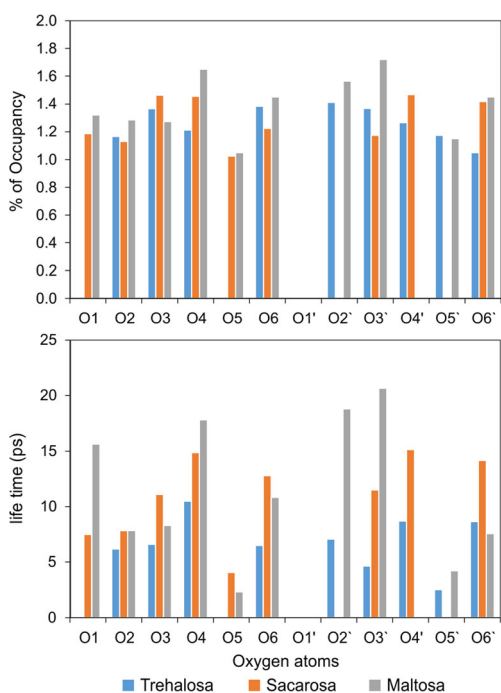

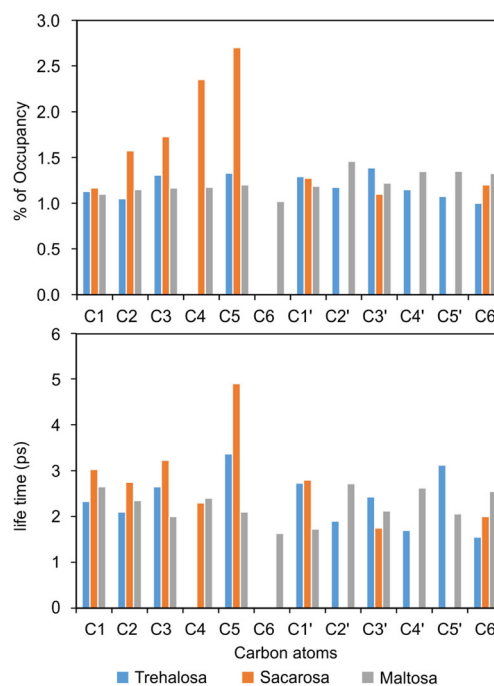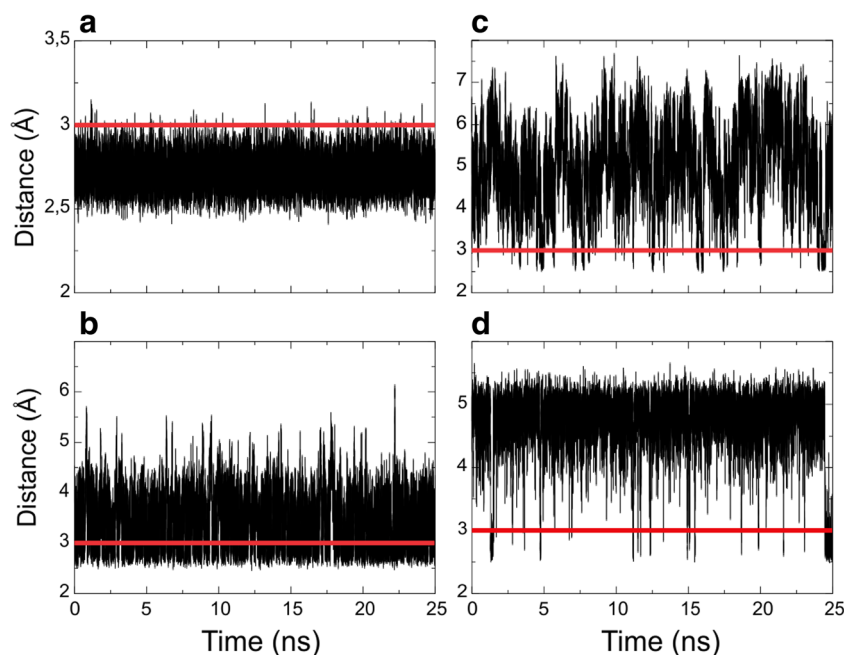**Fig. 6.** Average lifetimes and % of occupancy of O-H⋯O HBs for each O atom

Fig. 7 Average lifetimes and % of occupancy of C-H⋯O HBs for each C atom

Fig. 8. Trajectories of the main O/C···O distances corresponding to the intramolecular HBs. Sucrose: **a** O1g···O3f, **b** O1f···O2g and **c** O5g···O6f. Maltose: **d** O2···O3'

HB between these atoms. From the topological analysis, two water molecules have been found to occupy locations nearly identical to those in the dihydrate structures. A water molecule connects O2 and O4' atoms (Fig. 9a, see also Fig. 3b in static study as a reference) through a water bridge: O2···H-Ow-H···O4'. Whereas in the crystal structure O4' acts a proton donor: O2···H-Ow···H-O4'. The second water molecule adopts the same position than that found in the dihydrate-2. That is, the water molecule forms a bifunctional HB by acting as a proton donor in a conventional Ow-H···O HB and, simultaneously, as a proton acceptor in a, C-H···Ow HB: O5···H-Ow···H-C1'. In addition, this water molecule is also involved in a bifurcated HB as a double proton donor, to the O5 and O6 oxygens. This communion between static and dynamic study could support the water entrapment hypothesis, which establishes that sugars concentrate residual water molecules close to the biostructure, thereby preserving to a large extent its solvation and native properties [63–65].

On the other hand, the intramolecular C5'-H···O2 HB, which was found in the static study, has been also found in dilute solution (see Fig. 9a), however, the value of the density at BCP is slightly lower ($\rho(\mathbf{r}_c) = 0.0049$ au) than the value obtained by DFT calculation for the dihydrate forms (dihydrate 1, $\rho(\mathbf{r}_c) = 0.0068$ au and dihydrate 2 $\rho(\mathbf{r}_c) = 0.0126$ au) and for the anhydrous trehalose ($\rho(\mathbf{r}_c) = 0.0132$ au). It is important to note that no previous study has reported this intramolecular HB of trehalose in solution, and, to our opinion, it is very important as it would act as a folding mediator of trehalose against water scarcity.

Figure 8a–c shows the O1g···O3f, O1f···O2g and O5g···O6f distances, respectively, of oxygen atoms within a

sucrose molecule. The trace associated with the interaction between the O3f and O1g, fluctuates around a distance smaller than 3 Å along the simulation. Even though this fact would indicate the occurrence of an HB, in the QTAIM analysis, a CP between these atoms has not been found (see the molecular graph of Fig. 9b), so that the interatomic distance O3f and O1g is fixed by the geometry of the molecule. The O1f···O2g distance also reaches values lower than 3 Å along the entire simulation, although it fluctuates between 3 and 4 Å. This is consistent with the formation of the O2g-H···O1f HB (See Fig. 9b). The interaction between these two O atoms is also found in the crystal structure but with a reverse direction, as was previously shown by Immel and Lichtenhaler [66]. However, they found that a water molecule disrupts this HB by forming a water bridge. Results from MD in vacuum give evidence of the same intramolecular HB, being the occupancy for O2g-H···O1f and O1f-H···O2g HBs for about 76 and 13%, respectively. Regarding O5g···O6f distance; in Fig. 8c, it can be observed that although it reaches a value consistent with the formation of a HB at several points during the simulation, large fluctuations indicate that this HB is not stable. These results agree with the mobility about the glycosidic linkage observed for sucrose, a fact that prevents to form stable HBs for long times. In the molecular graph of Fig. 9b, several interactions, as a consequence of the changes around the glycosidic linkage, can be seen. In contrast to results previously reported [66] which stated that all intramolecular HBs are disintegrated in solution, in this study (anticlinal positive $\Phi = 104.3°$, $\Psi = -0.7°$) the following HBs and its corresponding values of $\rho(\mathbf{r}_c)$: O2g-H···O1f (0.02804 au), C1g-H···O5f (0.021608 au), C4f-H···O5g (0.008722 au), C6f–H···O5g
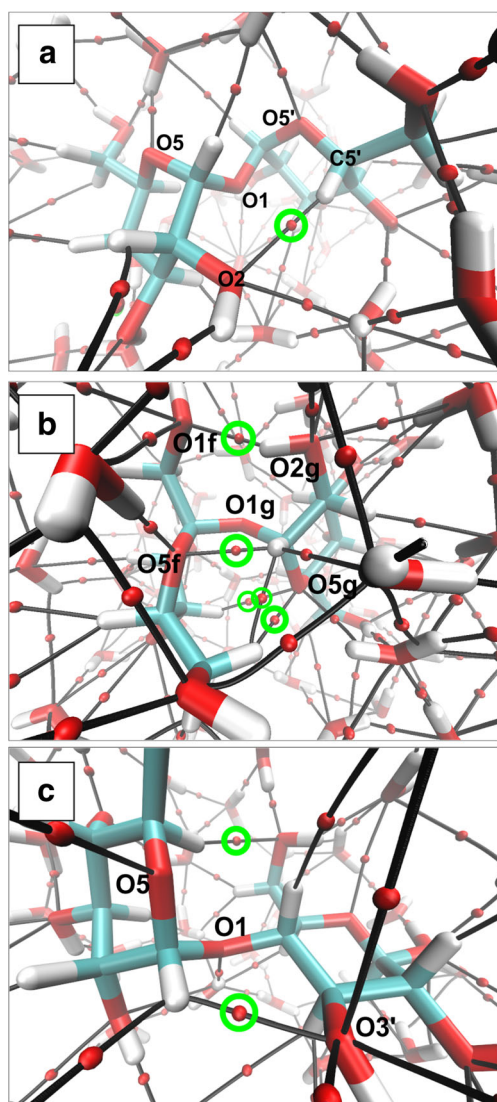
Fig. 9. Molecular graphs obtained from the MD simulations. *Green circles* indicate the intramolecular HBs **a** trehalose, **b** sucrose and **c** maltose

(0.007836 au) and C6f–H···H–C1g (0.007112 au) are observed. These results show the potential of QTAIM methodology to establish whether or not a bonding interaction occurs.

Finally, in Fig. 8d, the trajectory of the distance O2···O3', within a molecule of maltose, and in Fig. 9c, the molecular graph of the maltose in solution are shown. In Fig. 8d, it can be seen that the HB O2-H···O3' is formed just in some instances of the trajectory, which corresponds to a transition of the structure that is close to the crystal one. However, it seems that this conformation is not the preferable one in dilute aqueous solution. In the molecular graph of Fig. 9c, which corresponds to the most stable structure, two intramolecular HBs are observed: C1-H···O3' ($\rho(\mathbf{r}_c)$ = 0.01217 au) and C5-H···O6' ($\rho(\mathbf{r}_c)$ = 0.006759). They present values that agree well with this type of HB, and they show again the relevance of C-H···O

HBs since maltose prefers this configuration unlike the one found in the crystal which has stronger interactions.

Conclusions

Trehalose, sucrose and maltose in gaseous phase and infinitely dilute aqueous solution have been comparatively studied by electronic structure calculations and molecular dynamic simulations. A detailed analysis of HB interactions was carried out using QTAIM on wave functions obtained at B3LYP/6-311++G**. By using this technique in the gas phase, it has been found that the sucrose forms more intramolecular HBs than trehalose and maltose. In anhydrous and dihydrates trehalose a single internal HB, C-H···O is found. It would support the hypothesis of Conrad and de Pablo [62], who have suggested that the trehalose tends to fold over itself through HB when the presence of water molecules becomes scarce. We consider that this C-H···O, HB acts as a regulator of this folding. In the absence of water, the trehalose is folded and adopts a clam shell type conformation as observed in the crystal.

From MD simulation results, it has been seen that trehalose in aqueous solution has a greater conformational rigidity than sucrose and maltose concerning the glycosidic bond. Moreover, this bond is protected by an internal bifunctional HB.

It has also been observed that trehalose forms more HBs with water, both O-H···O type and C-H···O type. While occupancy and mean lifetime data indicate that these bonds are more labile, that is, they are formed and they break more rapidly than the other sugars. We think that this rapid exchange of HBs with surroundings water molecules prevents water molecules from reaching the degree of coordination typical of ice, i.e. four HBs per water molecule delaying ice formation.

References

1. Westh P, Ramlov H (1991) Trehalose accumulation in the tardigrade adorybiotus-coronifer during anhydrobiosis. J Exp Zool 258:303–311

2. Adams RP, Kendall E, Kartha KK (1990) Comparison of free sugars in growing and desiccated plants of *Selaginella lepidophylla*. Biochem Syst Ecol 18(2–3):107–110

3. Crowe JH, Crowe LM, Jackson SA (1983) Preservation of structural and functional activity in lyophilized sarcoplasmic reticulum. Arch Biochem Biophys 220:477–484

4. Lee SL, Hafeman AE, Debenedetti PG, Pethica BA, Moore DJ (2006) Solid-state stabilization of R-chymotrypsin and catalase with carbohydrates. Ind Eng Chem Res 45:5134–5147.c

5. Nakagaki M, Nagasse H, Ueda H (1992) Stabilization of the lamellar structure of phosphatidylcholine by complex-formation with trehalose. J Membr Sci 73:173–180

6. Xie GF, Timasheff SN (1997) The thermodynamic mechanism of protein stabilization by trehalose. Biophys Chem 64:25–43

7. Robinson CH (2001) Cold adaptation in Arctic and Antarctic fungi. New Phytol 151:341–353

8. Wang GM, Haymet ADJ (1998) Trehalose and other sugar solutions at low temperature: modulated differential scanning calorimetry (MDSC). J Phys Chem B 102:5341–5347

9. Green JL, Angell CA (1989) Phase relations and vitrification in saccharide-water solutions and the trehalose anomaly. J Phys Chem 93:2880–2882

10. Carpenter JF, Crowe JH (1989) An infrared spectroscopic study of the interactions of carbohydrates with dried proteins. Biochemistry 23:3916–3922

11. Roser B (1991) Trehalose a new approach to premium dried foods. Trends Food Sci Technol 2:166–169

12. Magazù S, Villari V, Faraone A, Maisano G, Heenan RK, King S (2002) α,α-trehalose-water solutions VI. A view of the structural and dynamical properties of OβG micelles in the presence of trehalose. J Phys Chem B 106:6954–6960

13. Debenedetti PG (1996) Metastable liquids: concepts and principles. Princeton University Press, Princeton

14. Debenedetti PG, Stanley HE (2003) Supercooled and glassy water. Phys Today 56:40–46

15. Pal SK, Peon J, Zewail AH (2002) Biological water at the protein surface: dynamical solvation probed directly with femtosecond resolution. Proc Natl Acad Sci U S A 99:1763–1768

16. Maillard LC (1912) Action des acides amines sur les sucres: formation des melanoidines par voie methodique. comptes rendus Acad Sci paris 154:66–68

17. Crowe JH, Crowe LM, Oliver AE, Tsvetkova N, Wolkers W, Tablin F (2001) The trehalose myth revisited: introduction to a symposium on stabilization of cells in the dry state. Cryobiology 43:89

18. Wang W (1999) Instability, stabilization and formulation of liquid protein pharmaceuticals. Int J Pharm 185:129

19. Haydon C (2000) SPC, Soap, Perfum. Cosmet 73:39

20. Villarreal MA, Díaz SB, Disalvo EA, Montich GG (2004) Molecular dynamics simulation study of the interaction of trehalose with lipid membranes. Langmuir 20:7844–7851

21. Pereira CS, Hünenberger PH (2006) Interaction of the sugars trehalose, maltose and glucose with a phospholipid bilayer: a comparative molecular dynamics study. J Phys Chem B 110:15572–15581

22. Francia F, Dezi M, Mallardi A, Palazzo G, Cordone L, Venturoli G (2008) Protein-matrix coupling/uncoupling in "dry" systems of photosynthetic reaction center embedded in trehalose/sucrose: the origin of trehalose peculiarity. J Am Chem Soc 130:10240–10246

23. Curtis JE, Dirama TE, Carri GA, Tobias DJ (2006) Inertial suppression of protein dynamics in a binary glycerol-trehalose glass. J Phys Chem B 110:22953–22956

24. Bellavia G, Giuffrida S, Cottone G, Cupane A, Cordone L (2011) Protein thermal denaturation and matrix glass transition in different protein-trehalose-water systems. J Phys Chem B 115:6340–6346

25. Buera P, Schebor C, Elizalde B (2005) Effects of carbohydrate crystallization on stability of dehydrates foods and ingredient formulations. J Food Eng 67:157–165

26. Lerbret A, Affouard F, Hédoux A, Krenzlin S, Siepmann J, Bellissent-Funel M-C, Descamps M (2012) How strongly does trehalose interact with lysozyme in the solid state? Insights from molecular dynamics simulation and inelastic neutron scattering. J Phys Chem B 116:11103–11116

27. Olsson C, Jansson H, Swenson J (2016) The role of trehalose for the stabilization of proteins. J Phys Chem B 120:4723–4731

28. Bader RFW (1990) Atoms in molecules, A Quantum Theory. Clarendon Press, Oxford

29. Weinhold F (1998) Natural bond orbital methods. In: Schleyer PVR, Allinger NL, Clark T, et al. (eds) Encycl. Comput. Chem. Wiley, Chichester, pp. 1792–1811

30. Brown GM, Rohrer DC, Berking B, Beevers CA, Gould RO, Simpson R (1972) The crystal structure of α,α-trehalose dihydrate from three independent x-ray determinations. Acta Cryst 28:3145

31. Taga T, Senma M, Osaki K (1972) The crystal and molecular structure of trehalose dihydrate. Acta Crystallogr Sect B Struct Crystallogr Cryst Chem 28:3258–3263

32. Brown GM, Levy HA (1973) Further refinement of the structure of sucrose based on neutron-diffraction data. Acta Crystallogr Sect B Struct Crystallogr Cryst Chem 29:790–797

33. Gres SME, Jeffrey GA (1977) A neutron diffraction refinement of the crystal structure of β-maltose monohydrate. Acta Crystallogr Sect B Struct Crystallogr Cryst Chem 33:2490–2495

34. Becke AD (1993) Density-functional thermochemistry. III. The role of exact exchange. J Chem Phys 98:5648

35. Lee C, Yang W, Parr RG (1988) Development of the Colle-Salvetti correlation-energy formula into a functional of the electron density. Phys Rev B 37:785–789

36. Frisch MJ, Trucks GW, Schlegel HB, Scuseria GE, Robb MA, Cheeseman JR, Montgomery JA Jr, Vreven T, Kudin KN, Burant JC, Millam JM, Iyengar SS, Tomasi J, Barone V, Men-nucci B, Cossi M, Scalmani G, Rega N, Petersson GA, Nakat-suji H, Hada M, Ehara M, Toyota K, Fukuda R, Hasegawa J, Ishida M, Nakajima T, Honda Y, Kitao O, Nakai H, Klene M, Li X, Knox JE, Hratchian HP, Cross JB, Bakken V, Adamo C, Jaramillo J, Gomperts R, Stratmann RE, Yazyev O, Austin AJ, Cammi R, Pomelli C, Ochterski JW, Ayala PY, Morokuma K, Voth GA, Salvador P, Dannenberg JJ, Zakrzewski VG, Dapprich S, Daniels AD, Strain MC, Farkas O, Malick DK, Rabuck AD, Raghavachari K, Foresman JB, Ortiz JV, Cui Q, Baboul AG, Clifford S, Cioslowski J, Stefanov BB, Liu G, Liashenko A, Piskorz P, Komaromi I, Martin RL, Fox DJ, Keith T, Al-Laham MA, Peng CY, Nanayakkara A, Challacombe M, Gill PMW, Johnson B, Chen W, Wong MW, Gonzalez C, Pople JA (2004) Gaussian 03, Revision D.01. Gaussian, Inc., Wallingford

37. NBO (Version 3.1) Glendening ED, Badenhoop JK, Reed AE, Carpenter JE, Weinhold F, Theoretical Chemistry Institute, University of Wisconsin, Madison, WI

38. AIMAll (Version 11.12.19), Keith TA, TK Gristmill Software, Overland Park KS, USA, 2011 (aim.tkgristmill.com)

39. Lu T, Chen F (2012) Multiwfn: a multifunctional wavefunction analyzer. J Comp Chem 33:580–592

40. Jorgensen WL, Chandrasekhar J, Madura JD, Impey RW, Klein ML (1983) Comparison of simple potential functions for simulating liquid water. J Chem Phys 79:926

41. Bayly CI, Cieplak P, Cornell WD, Kollman APA (1993) Well-behaved electrostatic potential based method using charge restraints for deriving atomic charges: the RESP model. J Phys Chem 97:10269–10280

42. Case DA, Darden TA, Cheatham III TE, Simmerling CL, Wang J, Duke RE, Luo R, Walker RC, Zhang W, Merz KM, Roberts B, Wang B, Hayik S, Roitberg A, Seabra G, Kolossváry I, Wong KF, Paesani F, Vanicek J, Liu J, Wu X, Brozell SR, Steinbrecher T, Gohlke H, Cai Q, Ye X, Wang J, Hsieh M-J, Cui G, Roe DR, Mathews DH, Seetin MG, Sagui C, Babin V, Luchko T, Gusarov S, Kovalenko A, Kollman PA (2010) AMBER 11. University of California, San Francisco

43. Izaguirre JA, Catarello DP, Wozniak JM, Skeel RD (2001) Langevin stabilization of molecular dynamics. J Chem Phys 114:2090

44. Ryckaert J-P, Ciccotti G, Berendsen HJ (1977) Numerical integration of the cartesian equations of motion of a system with constraints: molecular dynamics of n-alkanes. J Comput Phys 23: 327–341

45. Essmann U, Perera L, Berkowitz ML, Darden T, Lee H, Pedersen LG (1995) A smooth particle mesh Ewald method. J Chem Phys 103:8577

46. Nagase H, Ogawa N, Endo T, Shiro M, Ueda H, Sakurai M (2008) Crystal structure of an anhydrous form of trehalose: structure of water channels of trehalose polymorphism. J Phys Chem B 112: 9105–9111

47. Jeffrey GA, Nanni R (1985) The crystal structure of anhydrous α, α-trehalose at -150°. Carbohydr Res 137:21–30

48. Nunes SCC, Jesus AJL, Moreno MJ, Eusébio MES (2010) Conformational preferences of α,α-trehalose in gas phase and aqueous solution. Carbohydr Res 345:2048–2059

49. Boyd RJ, Choi SC (1986) Hydrogen bonding between nitriles and hydrogen halides and the topological properties of molecular charge distributions. Chem Phys Lett 129:62–65

50. Carroll MT, Bader RFW (1988) An analysis of the hydrogen bond in BASE-HF complexes using the theory of atoms in molecules. Mol Phys 65:695–722

51. Popelier PLA (1998) Characterization of a dihydrogen bond on the basis of the electron density. J Phys Chem A 102:1873–1878

52. Tvaroŝka I, Bleha T (1989) Advances in carbohydrate chemistry and biochemistry Volume 47

53. Choi Y, Cho KW, Jeong K, Jung S (2006) Molecular dynamics simulations of trehalose as a "dynamic reducer" for solvent water molecules in the hydration shell. Carbohydr Res 341:1020–1028

54. Bonanno G, Noto R, Fornili SL (1998) Water interaction with α,α-trehalose: molecular dynamics simulation. J Chem Soc Faraday Trans 94:2755–2762

55. Branca C, Magazú S, Maisano G, Migliardo F, Migliardo P, Romeo G (2001) α,α-Trehalose/water solutions. 5. Hydration and viscosity in dilute and semidilute disaccharide solutions. J Phys Chem B 105: 10140–10145

56. Engelsen SB, Monteiro C, Hervé de Penhoat C, Pérez S (2001) The diluted aqueous solvation of carbohydrates as inferred from molecular dynamics simulations and NMR spectroscopy. Biophys Chem 93:103–127

57. Engelsen SB, Pérez S (2000) Unique similarity of the asymmetric trehalose solid-state hydration and the diluted aqueous-solution hydration. J Phys Chem B 104:9301–9311

58. Bordat P, Lerbret A, Demaret J-P, Affouard F, Descamps M (2004) Comparative study of trehalose, sucrose and maltose in water solutions by molecular modelling. Europhys Lett 65:41–47

59. Pomata MHH, Sonoda MT, Skaf MS, Elola MD (2009) Anomalous dynamics of hydration water in carbohydrate solutions. J Phys Chem B 113:12999–13006

60. Winther LR, Qvist J, Halle B (2012) Hydration and mobility of trehalose in aqueous solution. J Phys Chem B 116:9196–9207

61. Pagnotta SE, Mclain SE, Soper AK, Bruni F, Ricci MA (2010) Water and trehalose: how much do they interact with each other? J Phys Chem B 114:4904–4908

62. Conrad PB, de Pablo JJ (1999) Computer simulation of the cryoprotectant disaccharide α,α-trehalose in aqueous solution. J Phys Chem A 103:4049–4055

63. Belton PS, Gil AM (1994) IR and Raman-spectroscopic studies of the interaction of trehalose with hen egg-white lysozyme. Biopolymers 34:957–961

64. Cottone G, Ciccotti G, Cordone L (2002) Protein-trehalose-water structures in trehalose coated carboxy-myoglobin. J Chem Phys 117:9862–9866

65. Lins R, Pereira C, Hünenberger P (2004) Trehalose-protein interaction in aqueous solution. Proteins 55:177–186

66. Immel S, Lichtenthaler FW (1995) The conformation of sucrose in water: a molecular dynamics approach. Liebigs Ann 1995:1925–1937